2010 IEEE International Conference on Robotics and Automation
Anchorage Convention District
May 3-8, 2010, Anchorage, Alaska, USA

Spectral Scan Matching and Its Application to Global Localization for Mobile Robots

Soonyong Park and Sung-Kee Park

Abstract— This paper presents a new scan matching method for mobile robot localization. The proposed method is based on a spectral technique, which finds consistent correspondences between two range scans without any initial alignment while considering how well their associated pairwise geometric relationships are satisfied. Based on the scan matching method, we also suggest a strategy for global localization in indoor environments, which is applicable to both grid maps and topological maps having metric information. The feasibility of the proposed methods is demonstrated by experimental results.

I. Introduction

In order to navigate safely and reliably, a mobile robot must be able to estimate its pose (position and rotation). One possible way to achieve this functionality is to use range scan matching, which is to estimate the relative pose between two successive locations by maximizing the overlap between an input scan and a reference scan obtained at each location. One of the major differences between the existing scan matching algorithms is the usage, or not, of an initial alignment (rotation and translation) between two scans. As described in [1], the scan matching methods can be classified into two types: sequential matching and global matching.

The sequential scan matching compares two successive scans with an initial assumption of alignment between them, in which the initial value is typically obtained by dead reckoning in advance. In a manner of iterative search beginning at the initial alignment, it finds an optimal alignment so that the matching errors between two scans are minimized. When a bad initial alignment is given, however, the sequential scan matching might fail to align two scans because the initial value is able to lead the matching result to a local minimum. The iterative closest point (ICP) method [2], which is a popular algorithm for matching sets of points or free-form curves and surfaces, uses Euclidean distance to evaluate the matching error between two scans. The LM-ICP method [3] uses the Levenberg-Marquardt algorithm. The matching error is directly minimized using the sum of squares of nonlinear functions. The iterative dual correspondence (IDC) method [4] solves the matching problem by searching the translation component and the rotation component separately. These methods are applicable to unstructured environments including arbitrary shapes such as free-form curves.

On the other hand, the global scan matching does not require an initial alignment, but it needs to detect polygonal features such as corners, curves, or lines. Therefore, it is difficult to use the global scan matching in unstructured environments where such features cannot be detected. The CCF method [5] matches two scans using the normalized cross correlation between angle histograms of the scans as well as x and y histograms. The Hough method [6] matches two scans with the lines extracted from the scans using the Hough transform. These methods are hard to be applicable in the case that the range scan contains a number of short line segments or curves. The curvature method [7] matches two scans using the adaptive curvature function which divides the scans into curve segments and line segments. This method needs the process for estimating the curvature function, and it is hard to provide a good result in the case that the scan includes many short arbitrary segments. The signature method [1] extracts Euclidean invariant signatures from the scan, and it uses a geometric hashing scheme to match two scans. This method, however, requires that the scan contains curved objects.

The Monte Carlo localization method [8] has been most widely used to both local pose tracking and global localization approaches. When it is applied to global localization, the samples are uniformly spread over the whole map since the initial robot pose is not given. In order to obtain a reliable result of pose estimation, the robot should move around its environment until all the samples converge into a local area. However, such movement is frequently inefficient and cumbersome. Furthermore, the Monte Carlo localization have some limitations in which it could fail to track the robot's position if the number of samples is insufficient, and its most applications are restricted to metric map such as grid map.

In this paper we propose a new scan matching method called the spectral scan matching (SSM). The proposed method is a kind of global scan matching, and can be used in both polygonal and non-polygonal environments without an initial alignment. It is also applicable even if unknown dynamic objects exist or the scan data are partially corrupted because it uses the whole scan data instead of a few extracted features.

We also suggest a global localization method which uses the framework of spectral scan matching. By taking the advantage of the spectral scan matching, it can avoid requiring an initial pose or any added movements such as in the Monte Carlo localization. Basically, the proposed localization method works in a topological map of which all nodes have 360° laser range scans obtained at their posi-

This research was performed for the Intelligent Robotics Development Program, one of the 21st Century Frontier R&D Programs funded by the Ministry of Knowledge Economy of Korea.

Soonyong Park and Sung-Kee Park are with the Cognitive Robotics Center at the Korea Institute of Science and Technology (KIST), 39-1 Hawolgok-dong, Sungbuk-gu, Seoul, Korea.
{scipio77,skee}@kist.re.kr

tions. In order to be applicable to a grid map, we extract the generalized Voronoi diagram (GVD) [9] from the grid map.

The rest of this paper is organized as follows. Section 2 proposes the spectral scan matching method, and a method to build a topological map from a grid map is described in Section 3. Section 4 presents a strategy for global localization using SSM. Experimental verifications are shown in section 5 and some concluding remarks are given in Section 6.

II. Spectral Scan Matching

The spectral scan matching consists of two stages. First, a spectral technique [10] is used to find geometrically consistent correspondences by using pairwise geometric relationships between scan points. And second, a RANSAC-based least squares fitting method [11] is used to estimate the robot pose.

A. Pairwise Geometric Relationships

We suppose the robot starts at location R_{ref} and acquires a scan S_{ref}. The robot then moves to a new location R_{new} and takes another scan S_{new}. Let $S_{ref} = \{\mathbf{p}_1, \ldots, \mathbf{p}_n\}$ and $S_{new} = \{\mathbf{r}_1, \ldots, \mathbf{r}_m\}$ be the sets of scan points acquired in each given location. Let $\mathbf{q} = [t_x, t_y, \theta]^T$ be the relative location of R_{new} with respect to R_{ref}. Let Q be a set of correspondence pairs (i, i'), where $i \in S_{ref}$ and $i' \in S_{new}$. Fig. 1 (a) shows the simple features used in our approach. At every scan point $\mathbf{p}_i$, the tangent direction $\mathbf{u}_i$ is computed. We use the approximate estimate:

$$\mathbf{u}_i = \frac{\mathbf{p}_{i+1} - \mathbf{p}_{i-1}}{\left\| \mathbf{p}_{i+1} - \mathbf{p}_{i-1} \right\|} \tag{1}$$

Fig. 1 (b) shows the pairwise geometric relationships between two scan points. For a pair of scan points (i,j), we compute their distance-angular relationship:

$$d_{ij} = \left\| \mathbf{p}_i - \mathbf{p}_j \right\| , \ \theta_{ij} = arccos\left(\mathbf{u}_i \cdot \mathbf{u}_j \right) \tag{2}$$

where d_{ij} is the distance between them and θ_{ij} is the angle between their tangent directions. We consider the same type of pairwise relationship for the pair of (i',j') which are matched with (i,j). We can then define a vector describing the geometric deformations between the scan points (i,j) and their matched points (i',j'):

$$\mathbf{g}_{ij}\left(i', j'\right) = \left[1 \quad \left(d_{ij} - d_{i'j'} \right)^2 \quad \left(\theta_{ij} - \theta_{i'j'} \right)^2 \right]^T \tag{3}$$

For every pair of possible correspondences $a = (i, i')$ and $b = (j, j')$, we define a pairwise potential G_{ab}. This pairwise potential captures the degree to which the two correspondences are compatible geometrically, and it is represented in the form of a logistic regression classifier [12]:

$$G_{ab} = \frac{1}{\left(1 + exp(-\mathbf{w}^T \mathbf{g}_{ij}(i', j')) \right)} \tag{4}$$

where $\mathbf{g}_{ij}(i', j')$ is the geometric deformation vector and $\mathbf{w}$ is a regression coefficient vector.

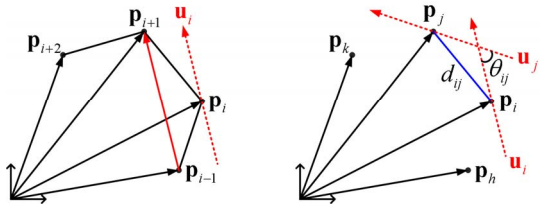

(a) (b)

Fig. 1. (a) Simple features: scan point $\mathbf{p}_i$ and its tangent direction $\mathbf{u}_i$. (b) Pairwise geometric relationships: distance-angular relationships (d_{ij} and θ_{ij}) between two scan points $\mathbf{p}_i$ and $\mathbf{p}_j$.

B. Detection of Consistent Correspondences

Our matching method is based on a spectral technique [10], which considers the matching problem as a quadratic assignment problem. It finds the set Q of correspondence pairs (i, i') that maximizes the matching score:

$$E = \sum_{a,b \in Q} \mathbf{x}(a)\mathbf{x}(b)\mathbf{G}(a,b) = \mathbf{x}^T \mathbf{G} \mathbf{x} \tag{5}$$

where $\mathbf{x}$ is binary indicator vector with an element for each correspondence pair $a = (i, i')$ such that $\mathbf{x}(a) = 1$ if scan point i in S_{ref} is matched with i' in S_{new} (*e.g.* $a \in Q$) and 0 otherwise. Q is a subset of the set L of all tentative correspondences. $\mathbf{G}$ is an affinity matrix which consists of pairwise potential: $\mathbf{G}(a, b) = G_{ab}$. It is built symmetrically with every pair of correspondences $a, b \in L$. The diagonal elements of the affinity matrix, G_{aa}, is set to 0, and off-diagonal elements are computed by (4). In addition, if the geometric deformation between (i, j) and (i', j') is too large or if they do not satisfy the mapping constraints (*e.g.* $i = j$ and $i' \neq j'$), we set $G_{ab} = 0$. The optimal solution for (5) is the assignment $\mathbf{x}^*$ that maximizes the matching score E:

$$\mathbf{x}^* = argmax(\mathbf{x}^T \mathbf{G} \mathbf{x}) \tag{6}$$

According to the Rayleigh quotient theorem [13], we can obtain $\mathbf{x}^*$ by taking the eigenvector associated with the largest eigenvalue of $\mathbf{G}$. The elements of $\mathbf{x}^*$ will be in [0, 1] by Perron-Frobenius theorem [14]. This is the relaxed and continuous vector, so we then binarize $\mathbf{x}^*$ to find discrete assignments. The binarization is performed by repeating the following three steps:

Step – 1: Find $a^* = argmax_{a \in L}(\mathbf{x}^*(a))$. If $\mathbf{x}^*(a^*) = 0$ stop the binarization. Otherwise set $\mathbf{x}(a^*) = 1$ and remove a^* from L.

Step – 2: Remove from L all potential correspondences which conflict with $a^* = (i, i')$. These have the form of $(i, *)$ or $(*, i')$.

Step – 3: If L is empty, return the solution $\mathbf{x}$. Otherwise go back to Step 1.

C. Pose Estimation

We now estimate the robot pose $\mathbf{q} = [t_x, t_y, \theta]^T$ with the RANSAC-based least squares estimation method [11] as follows:

Step – 1: Randomly select two correspondence pairs (i, i') and (j, j') from Q.

Step – 2: Compute tentative robot pose. We can obtain two equations with three unknowns:

$$t_x = x_i - x_{i'}cos\theta + y_{i'}sin\theta$$
$$t_y = y_i - x_{i'}sin\theta - y_{i'}cos\theta \quad (7)$$

where (x_i, y_i) and $(x_{i'}, y_{i'})$ are the positions of i and i', respectively. With two correspondence pairs (i, i') and (j, j'), we have

$$Acos\theta - Bsin\theta = C$$
$$Asin\theta + Bcos\theta = D \quad (8)$$

where $A = (x_{i'} - x_{j'})$, $B = (y_{i'} - y_{j'})$, $C = (x_i - x_j)$, $D = (y_i - y_j)$. Solving (7) and (8), we obtain $\theta = arctan((AD - BC)/(AC + BD))$ and substituting this into (7) gives a tentative pose.

Step – 3: Check all the correspondence pairs in Q, which support this pose. We first compute relative positions of all i' with respect to this pose:

$$x_{i'}' = x_{i'}cos\theta - y_{i'}sin\theta + t_x$$
$$y_{i'}' = x_{i'}sin\theta + y_{i'}cos\theta + t_y \quad (9)$$

and then compute distances between (x_i, y_i) and $(x_{i'}', y_{i'}')$. (i, i') supports this pose if the distance is smaller than a threshold value.

Step – 4: Repeat Step 1 through Step 3 K times. We then choose the pose that has the highest number of supports, and proceed with the least squares minimization for the inliers that support this pose and obtain a better estimate for the pose.

III. Building a Topological Map from a Grid Map

The proposed global localization method can be applied in a grid map. The key idea is to first build a topological map from a grid map. To build a topological map, we extract the generalized Voronoi diagram (GVD) [9] from the free space of a grid map and detect node positions on the GVD. In order to construct the GVD, we employ the brushfire algorithm [9, 15] of which output is a discrete map where each pixel in the grid has a value equal to the distance to the closest point on the closest obstacle. A node on the GVD denotes the branch point at which three or more arcs meet (Fig. 5). We call it by a branch node.

Virtual range scans are then extracted at all node positions. Since the virtual range scans approximate real range scans of the robot, it is possible to use them in our localization method. We use a ray-casting (ray-tracing) operation to extract the virtual range scans.

Table 1 depicts the algorithm for ray-casting operation. We denote the number of scan ray within a set of range beams Z_q by K. In order to simulate the range beams in the global reference frame of the map m, we need to know in the global coordinate system where the coordinate system of robot is, where on the robot the range beam z^k stems from, and where it points. Let $\boldsymbol{q} = [x, y, \theta]^T$ be the pose of robot in the global coordinate system. The pose of laser range finder fixed on the robot is defined relative to the coordinate system of robot, and it is denoted by $[x_{sens}, y_{sens}, \theta_{sens}]^T$. We set the pose of laser range finder with respect to the global coordinate system as $[q_x, q_y, \theta_q]^T$. θ_k denotes the angular orientation of *k-th* range beam relative to the coordinate system of laser range finder.

Table 1. Algorithm for ray-casting (ray-tracing) operation

1	Algorithm RAY-CASTING;
2	$Z_q = \{z_q^0, \ldots, z_q^K\}$
3	begin
4	$q_x = x + x_{sens}cos\theta - y_{sens}sin\theta$ $q_y = y + x_{sens}sin\theta + y_{sens}cos\theta$ $\theta_q = \theta + \theta_{sens}$
5	$\theta_k = 0$ $(k = 0)$
6	for $k = 0$ to K do
7	$z_q^k = 0$
8	while $m(x_q^k, y_q^k) \neq 0$ do
9	$z_q^k = z_q^k + \Delta d$
10	$\begin{pmatrix} x_q^k \\ y_q^k \end{pmatrix} = \begin{pmatrix} q_x \\ q_y \end{pmatrix} + \begin{pmatrix} cos\theta_t & -sin\theta_t \\ sin\theta_t & cos\theta_t \end{pmatrix} \begin{pmatrix} z_q^k cos\theta_q \\ z_q^k sin\theta_q \end{pmatrix}$
11	end while;
12	$\theta_{k+1} = \theta_k + \Delta\theta$
13	end for;
14	end;

For every z_q^k in Z_q, the length of each range beam increases as Δd until it meets an occupied grid cell of the map m. We denote by $m(x_q^k, y_q^k)$ the occupied grid cell that is hit by the range beam z_q^k. After *k-th* range beam obtains a measurement value, next range beam z_q^{k+1} starts to detect an occupied grid cell and its angular orientation θ_{k+1} is set by adding $\Delta\theta$ to θ_k.

IV. Global Localization Using SSM

Global localization is to estimate robot pose in a previously learned map without knowing initial pose. It gives the robot abilities to deal with initialization and recovery from kidnapping problem.

Fig. 2 shows the flowchart of proposed global localization system. From a given grid map, the GVD of the free space is constructed. The branch nodes on the GVD are detected and the virtual range scans at all node positions are extracted. Pairwise geometric relationships are constructed for range scan of each node. When the robot performs global localization, it obtains its pose relative to the coordinate system of the nearest node.

The global localization process consists of two stages: *coarse localization* and *fine localization*. The coarse localization employs the spectral matching technique [10], and its results are given as the candidate nodes for the following fine localization. Each candidate node has the set of matched scan points with the range scan for localization. Using the RANSAC-based least squares estimation method [11], the fine localization determines the correct node among the candidate nodes and estimates robot pose with respect to the correct node.

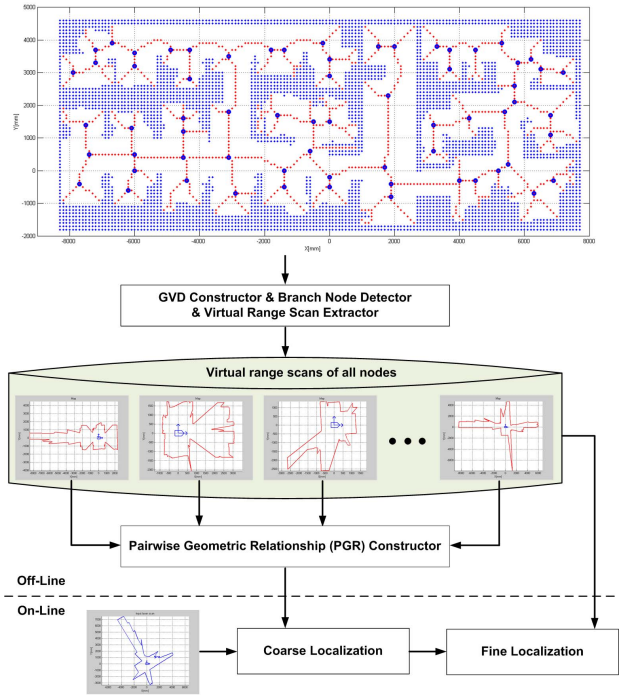

Fig. 2. Flowchart of our global localization system.

A. Coarse Localization

In this stage, the degree of similarity between the range scan of each node and the query range scan for localization is evaluated by computing the spectral matching score in (5) with the optimal solution of (6). We assume that the similarity value is an indication of the relevance between the node and the query range scan. Thus, each node is ranked in accordance with the similarity value.

The nodes whose similarity values rank in the top N are considered as the candidate nodes where the robot is expected to be located, and they will be taken as the input of the next stage. In this paper, we set $N = 5$.

B. Fine Localization

Localization at this stage is carried out based on the results of the coarse localization. Fine localization is realized with two steps. First, the robot poses relative to all candidate nodes are computed with the RANSAC-based least squares estimation method. Second, the vicinity score is calculated for each candidate node. Finally, the candidate node that gets the largest vicinity score is determined as the correct node.

Spatial continuity is an inherent nature of geographic phenomena. It is the propensity for nearby locations to possess similar attributes [16]. Thus, it is also clear that the closer the current location of the robot is to the location of the correct node, the greater the degree of similarity between the range scan for localization and that of the correct node. In this paper, the spatial continuity is quantitatively expressed as the vicinity score M which evaluates the similarity between the two range scans [10]:

$$M\left(S_{node}, S_{robot}\right) = \sum_i m_i$$

$$m_i = \begin{cases} 4.5 - \dfrac{dist\left(\mathbf{p}_i, \mathbf{r}_i\right)^2}{2\sigma_d^2} & if\ dist\left(\mathbf{p}_i, \mathbf{r}_i\right) < 3\sigma_d \\ 0 & otherwise \end{cases} \tag{10}$$

where M is the vicinity score between two range scans S_{node} and S_{robot}. $(\mathbf{p}_i, \mathbf{r}_i)$ is a corresponding pair where $\mathbf{p}_i \in S_{node}$ and $\mathbf{r}_i \in S_{robot}$. The function $dist(\ )$ computes the Euclidean distance between the scan points $\mathbf{p}_i$ and $\mathbf{r}_i$. The parameter σ_d controls the sensitivity of the measure m_i on deformation. The larger σ_d the more deformations between the two range scans we can adjust. In this paper, we set $\sigma_d = 50$ [mm]. The vicinity score M is always positive and increases as the deformation between corresponding pairs decreases.

V. Experimental Results

Our spectral scan matching and global localization methods have been tested and implemented in this section.

A. Spectral Scan Matching

The spectral scan matching method has been evaluated on the accuracy of pose estimates and its robustness with respect to errors due to deformation noise and ratio of outliers to inliers. To compare our SSM method with existing scan matching techniques, we chose the widely known IDC method [4] and CCF method [5].

The first experiment consisted of matching two scans acquired in the same robot location, $(t_x, t_y, \theta) = (0, 0, 0)$. One scan was composed of 362 points. The two scans differ from each other due to the sensor noise and the presence of dynamic objects in the robot surrounding. Next, we disturbed the second scan with white Gaussian noise $N(0, \sigma)$, and added n_O outliers by swapping x-y coordinates of scan points that were randomly selected in the second scan. We set $\sigma = 10$ and $n_O = 60$. The second scan was then applied to a random pose up to ±400[mm] in t_x and t_y, and up to ±30[°] in θ. The two scans which are misaligned with each other by a pose ($t_x = t_y = 400$[mm], $\theta = 30$[°]) are shown in Fig. 3 (a). The initial pose and misaligned pose are denoted by circles with arrows. The results of correcting the pose error and aligning the two scans with our method appear in Fig. 3 (b). We repeated the experiment 500 times in this scenario. Table 2 depicts the mean and standard deviations of the pose errors from the SSM, IDC, and CCF methods. It can be seen that the pose errors from SSM are quite small compared with the other two methods. These statistical results indicate that the proposed method is robust and accurate.

The second experiment evaluated the robustness of matching performance. The first scan used in the first experiment was applied as the first scan in the second experiment. We obtained the second scan by disturbing the first scan with white Gaussian noise, and then rotating and translating randomly, and next adding outliers in the same manner as the first experiment. Fig. 4 shows the performance curves of the

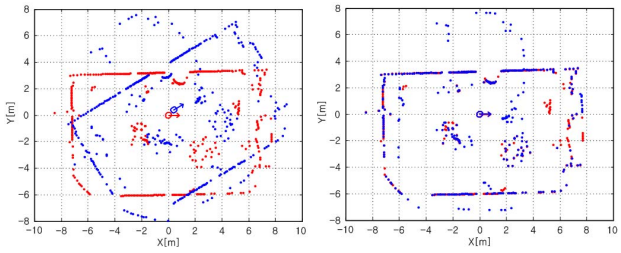

(a) (b)

Fig. 3. Two scans used in the evaluation experiment of SSM. Red points for the first scan and blue points for the second scan with outliers. (a) Misaligned two scans before scan matching. (b) Aligned two scans after scan matching.

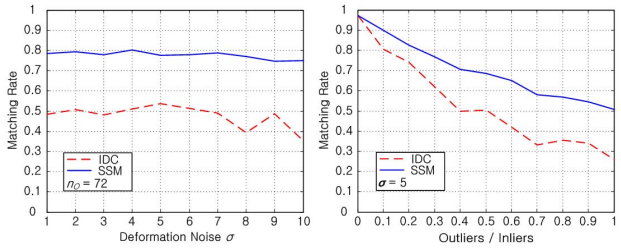

(a) (b)

Fig. 4. Performance curves for SSM method vs. IDC method. (a) 72 outliers, varying deformation noise. (b) Deformation noise $\sigma = 5$, varying ratio of outliers to inliers.

Table 2. Mean (μ) and standard deviation (σ) of estimated pose errors with SSM, IDC, and CCF methods.

	x error [mm]		y error [mm]		θ error [mm]	
	μ	σ	μ	σ	μ	σ
SSM	0.10	10.40	-0.30	7.09	0.02	0.10
IDC	2.90	207.16	-37.85	294.90	0.35	4.18
CCF	-84.40	95.58	-102.00	104.78	-0.53	8.13

SSM method vs. the IDC method. Both algorithms ran over 30 trials on the same problem scans for each parameter value on the x axis. The matching rates (correctly matched inliers/total inliers) were obtained by averaging the 30 tests. The proposed method proves to be more robust than the IDC method to deformation noises or the presence of outliers. This is because each correct correspondence can establish pairwise relationships with other correct correspondences even in the presence of pairwise relationships with incorrect correspondences.

B. Global Localization

We evaluated the global localization strategy with the grid map of our laboratory at International Cooperation Building in KIST. The size of the test environment was about 17[m] x 7[m]. From the grid map, we constructed the GVD using the brushfire algorithm and detected the branch nodes where three or more arcs meet (Fig. 5). The number of detected nodes was 66. The virtual range scans at the positions of all nodes were then extracted with the ray-casting operation.

Two types of experiments were conducted. The first evaluated the proposed global localization method in detail. The second evaluated the accuracy of estimated robot poses. The experiments were performed in the manner of simulation, i.e.

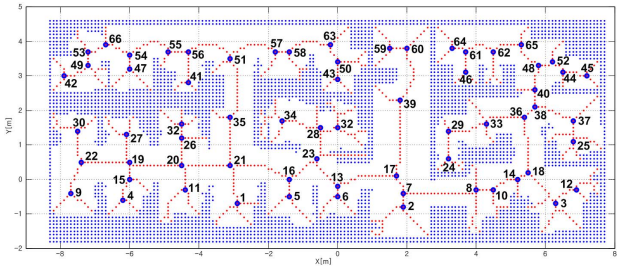

Fig. 5. GVD constructed from the grid map of our laboratory and the branch nodes extracted from it. The number of branch nodes is 66.

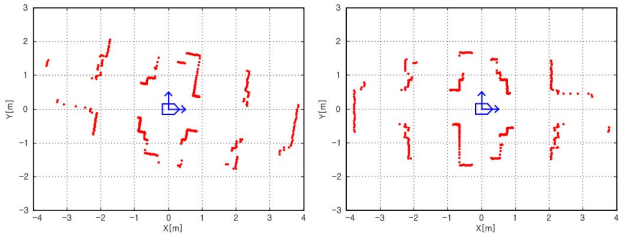

(a) (b)

Fig. 6. (a) Laser range scan for localization in a static situation. (b) Laser range scan extracted at node 20.

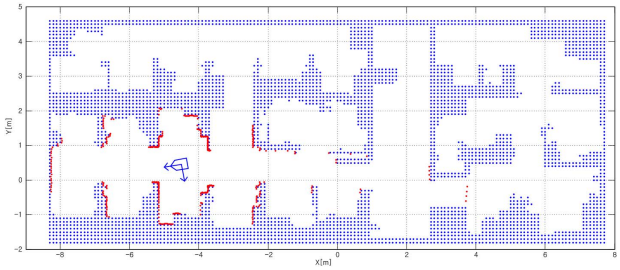

Fig. 7. Indication of global localization result on the grid map.

Table 3. Results of global localization performed with the scan in Fig. 6 (a).

Candidate node		20	19	21	15	51
Spectral matching score		9530.22	2964.30	2312.24	2261.81	1899.99
Vicinity score		771.46	589.35	596.19	507.48	297.01
Local pose	x_L [mm]	0.13	-93.56	-1327.98	-47.48	63.67
	y_L [mm]	76.13	-58.82	196.46	398.40	-1126.57
	θ_L [°]	-169.96	-166.42	-172.11	7.09	-81.77
Global pose	x_G [mm]	-4499.87	-6093.56	-4427.98	-6047.48	-3036.33
	y_G [mm]	476.13	441.18	596.46	398.41	2373.43
	θ_G [°]	-169.96	-166.42	-172.11	7.09	-81.77
Error	$\lvert t_x - x_G \rvert$	0.13	1593.56	72.02	1547.48	1463.67
	$\lvert t_y - y_G \rvert$	16.13	18.82	136.46	61.59	1913.43
	$\lvert \theta - \theta_G \rvert$	0.04	3.58	2.11	177.09	88.23

all laser range scan for localization tests were extracted at randomly selected positions on the grid map. Thus, we can know the ground truth values to compare with the results of localization tests.

The first experiment consisted of performing global localization at a random location. On the grid map in Fig. 5, we selected a random position and extracted virtual range scan. Fig. 6 (a) shows the virtual range scan extracted at the test location on the gird map. Since we chose the test position on the grid map, the ground truth pose was clearly known: $(t_x, t_y, \theta) = (-4500\ [\text{mm}], 460[\text{mm}], -170[°])$.

We performed the proposed global localization method with

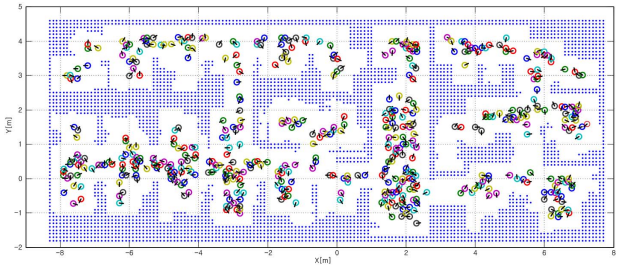

(a)

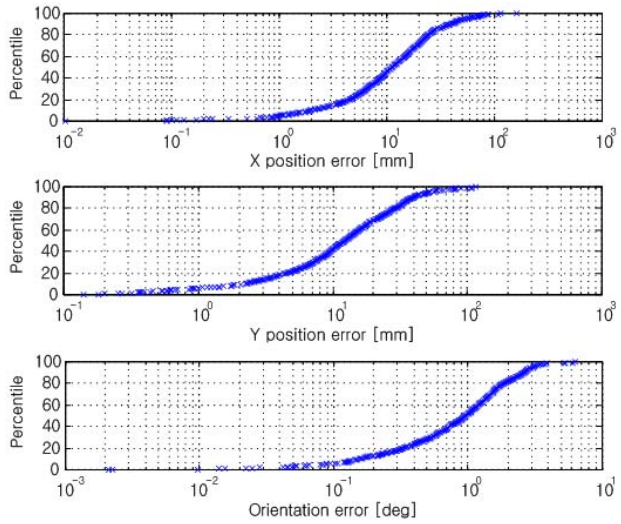

(b)

Fig. 8. (a) Localization results for different test locations in the grid map of our laboratory. (b) Error distribution for the localization results.

the virtual range scan in Fig. 6 (a). Table 3 shows the results of global localization. The local pose indicates the relative pose to the reference frame of each node. It can be transformed with respect to one global coordinates system (e.g. reference frame of the grid map) since the reference frame of each node is defined relative to the global coordinate system. We denote the transformed local pose as the global pose.

According to the spectral matching score, nodes 20, 19, 21, 15, and 51 were selected as the candidate nodes. Among them, node 20 obtained the largest spectral matching score as well as vicinity score. Furthermore, the error between the ground truth and the global pose defined through node 20 was the smallest. Therefore, node 20 was determined to be the correct node. Fig. 6 (b) shows the range scan of node 20. We can identify that the range scan for localization in Fig 6 (a) is very similar to the range scan of node 20 in Fig. 6 (b). Fig. 7 depicts the result of global localization on the grid map. We can also clearly see that the range scan for localization is remarkably matched with the grid map.

The second experiment focused on verifying the accuracy of the pose estimation in the grid map of our laboratory. For this experiment, a total of 500 different test positions were randomly chosen from the whole grid map. Unlike Monte Carlo localization [8], the robot did not need additional any motion behavior to localize. Fig. 8 (a) shows the global localization results for the test positions, indicating the robot's estimated position and orientation relative to its environment. Fig. 8 (b) shows error distribution diagrams, in which the mean and median errors were less than (16.77[mm], 17.91[mm], 1.19[°]) and (11.12[mm], 12.11[mm], 0.95[°]), respectively. As these figures demonstrate, the proposed localization algorithm gave a very satisfactory performance in experimental testing.

VI. Conclusions

In this paper, we proposed a new scan matching method which estimates robot pose without an initial alignment. This method finds consistent correspondences between two range scans, by considering how well their associated pairwise geometric relationships are satisfied. And on the basis of it, we suggested a global localization method that is applicable to both grid maps and topological maps having metric information. Our global localization method has a benefit such that it can estimate robot pose at current location without wandering motion. The experimental results showed that the proposed methods could be accurate and effective approaches to mobile robot navigation.

References

[1] M. Tomono, "A Scan Matching Method using Euclidean Invariant Signature for Global Localization and Map Building," *IEEE International Conference on Robotics and Automation*, 2004, pp. 866-871.

[2] Z. Zhang, "Iterative Point Matching for Registration of Free-Form Curves and Surfaces," *International Journal of Computer Vision*, vol. 13, no. 2, pp. 119-152, 1994.

[3] A. W. Fitzgibbon, "Robust Registration of 2D and 3D Point Sets," *Image and Vision Computing*, vol. 21, pp. 1145-1153, 2003.

[4] F. Lu and E. Milios, "Robot Pose Estimation in Unknown Environment by Matching 2D Range Scans," *IEEE Conference on Computer Vision and Pattern Recognition*, 1994, pp. 935-938.

[5] G. Weiss and E. Puttkamer, "A Map Based on Laserscans without Geometric Interpretation," *International Conference of Intelligent Autonomous Systems*, 1995, pp. 403-407.

[6] G. Grisetti, L. Iocchi, and D. Nardi, "Global Hough Localization for Mobile Robots in Polygonal Environments," *IEEE International Conference on Robotics and Automation*, 2002, pp. 353-358.

[7] P. Núñez, R. Vázquez-Martín, J.C. del Toro, A. Bandera, and F. Sandoval, "Natural landmark extraction for mobile robot navigation based on an adaptive curvature estimation," *Robotics and Autonomous Systems*, vol. 56, pp. 247-264, 2008.

[8] D. Fox, W. Burgard, F. Dellaert, and S. Thrun, "Monte Carlo Localization: Efficient Position Estimation for Mobile Robots," *National Conference on Artificial Intelligence*, 1999, pp. 896-091.

[9] H. Choset, K. Lynch, S. Hutchinson, G. Kantor, W. Burgard, L. Kavraki, and S. Thrun, *Principles of Robot Motion: Theory, Algorithms, and Implementation*, MIT Press, 2005.

[10] M. Leordeau and M. Hebert, "A Spectral Technique for Correspondence Problems using Pairwise Constraints," *International Conference on Computer Vision*, 2005, pp. 1482-1489.

[11] P. J. Rousseeuw and A. M. Leroy, *Robust Regression and Outlier Detection*, Wiley, 2003.

[12] S. Kumar, "Models for Learning Spatial Interactions in Natural Images for Context-Based Classification," PhD thesis, The Robotics Institute, Carnegie Mellon University, 2005.

[13] K. Lange, *Numerical Analysis for Statisticians*, Springer, 1999.

[14] R. A. Horn and C. R. Johnson, *Matrix analysis*, Cambridge University Press, 1985.

[15] J.-C. Latombe, *Robot Motion Planning*, Kluwer Academic Publishers, 1991.

[16] M. F. Goodchild, "Geographical information science," *International Journal of Geographical Information Systems*, vol. 6, no. 1, pp. 31-45, 1992.